ARCHIVES OF MECHANICS
Arch. Mech. **77** (4), 355–378, 2025, https://doi.org/10.24423/aom.4676

Characteristics of SH waves in multilayered piezoelectric semiconductor plates considering interfacial imperfection

Y. H. LUO, X. M. ZHANG, A. R. GAO*)

School of Mechanical and Power Engineering, Henan Polytechnic University, 454003, Jiaozuo, P.R. China, e-mail): gaoanru@outlook.com (corresponding author)*

The dispersion and attenuation characteristics of SH waves in piezoelectric semiconductor multilayered plates with imperfect interfaces are investigated using the improved Legendre orthogonal polynomial method. The field quantities of each layer are expanded into individual Legendre polynomials. By incorporating the interface conditions, the imperfect interface model is integrated into the Legendre polynomials associated with the imperfect interface layer. This method ultimately converts the complex wave partial differential equations into a generalized eigenvalue problem, thereby eliminating the redundant integration operations typical of traditional polynomial methods and allowing for the derivation of complete solutions throughout the entire wave frequency domain. The solutions are then plotted in three-dimensional frequency-complex wavenumber space, thus gaining much deeper insight into the nature of modes. The study encompasses cases ranging from a single-layer ZnO plate, which serves to validate the method, to bilayered and sandwiched piezoelectric semiconductor plates with imperfect interfaces. The effects of steady-state carrier concentration, imperfect interface coefficients, and stacking sequences on the phase velocity, dispersion, and attenuation curves of SH waves are illustrated. The findings can offer a theoretical foundation for controlling the wave characteristics of piezoelectric semiconductors and for the design of acoustic devices.

Key words: piezoelectric semiconductor, multilayered plate, SH wave, imperfect interface, Legendre orthogonal polynomial method, dispersion and attenuation.

1. Introduction

Piezoelectric semiconductor (PSC) is a type of functional material that exhibits multi-field coupling effects among mechanics, electricity, and carriers. It possesses the dual physical properties of piezoelectricity and semiconductivity, which endows it with broad application prospects in electronic devices such as high-frequency ultrasonic transducers, resonators, filters, and nanogenerators. The development and performance optimization of novel piezoelectric semiconductor devices require a deep understanding and mastery of the dynamic behaviors of piezoelectric semiconductor structures, particularly the characteristics of elastic wave propagation within these structures [1, 2]. Piezoelectric

semiconductors can convert mechanical vibrations or stress into electrical signals. Understanding how waves propagate in these materials allows for the design of more efficient energy harvesting devices.

The layered structure is a commonly used basic configuration in various piezoelectric and piezoelectric semiconductor devices, and its wave problems have been extensively studied [3, 4]. Xiao *et al.* [5] used the Chebyshev spectral element method to study the dispersion characteristics of guided waves in a multilayered magneto-electro-elastic curved panel, revealing the effects of the magnetoelectric effect, thickness-to-diameter ratio, and stacking sequence on the dispersion characteristics. Gao and Zhang [6] investigated guided wave propagation in anisotropic piezoelectric multilayered structures using the precise integration method of the Wittrick–Williams algorithm, and they illustrated the effects of boundary conditions, wave propagation direction, and thickness ratios on the behavior of guided waves. Using the state-vector approach, Chen *et al.* [7] investigated the propagation of harmonic waves in magneto-electro-elastic multilayered plates composed of PZT-5A, $BaTiO_3$, and $CoFe_2O_4$ materials, and Ezzin *et al.* [8] investigated the dispersion characteristics of Lamb waves in piezoelectric-piezomagnetic layered plates. Yang *et al.* [9] studied extensional waves in a composite plate of piezoelectric ceramics and semiconductors and discussed dispersion and dissipation due to semiconduction as well as wave amplification by an electric field. Gupta and Bhengra [10] investigated the SH wave in a multilayered orthotropic magnetoelastic medium using Haskell's matrix technique. Using the Legendre polynomial approach, Matar *et al.* [11] computed mode shapes of elastic waves in layered piezoelectric-piezomagnetic composites, and Othmani *et al.* [12, 13] investigated the characteristics of Lamb waves in piezoelectric semiconductor multilayered structures made of AlAs and GaAs and in the GaAs-FGPM-AlAs sandwich plate, considering only piezoelectricity without considering the semiconductor property. In the above studies, the interlayer interface is routinely assumed to be perfect; that is, displacements and tractions are continuous across the interface.

However, in practical applications, layered structures may exhibit microcracks or micropores at the interface, resulting in a decrease in mechanical strength and the formation of imperfect bonding. An imperfect interface refers to the connection between different material layers that is not perfectly continuous or bonded and contains certain defects or discontinuities. These defects may manifest as discontinuities in mechanical displacement, electric potential, stress, or electric field. Compared with ideal interfaces, imperfect interfaces cannot fully transmit stress or electric fields and usually require the introduction of additional interface parameters to describe their mechanical and electrical behaviors. Such imperfect interfaces are common in real-world applications, especially in micro/nano-electromechanical systems, where the fabrication process

may introduce interfacial defects. Imperfect interfaces can weaken the stiffness and continuity of the interface, leading to changes in wave propagation characteristics. The study of imperfect interfaces in piezoelectric semiconductor layered structures is crucial for optimizing the performance of devices such as sensors, transistors, and resonators. For example, imperfect interfaces can affect the reflection and transmission characteristics of elastic waves, thereby influencing the sensitivity and response speed of the devices. Therefore, it is essential to consider imperfect interfaces in the design and application of such structures.

The wave problem in multilayered structures with imperfect interfaces has attracted increasing attention from researchers in the past years. The effects of the interface imperfection on wave propagation in elastic bi-materials have been investigated in [14–16]. Nie *et al.* [17, 18] used the partial wave method to investigate the effect of an imperfect interface on the Lamb and SH waves in a double-layered plate composed of a piezoelectric layer and a piezomagnetic layer. Chaudhary *et al.* [19] studied SH wave propagation in a piezoelectric-piezomagnetic layered pre-stressed rotating cylindrical tube structure having an imperfect interface using an analytical technique. Kurt *et al.* [20] investigated the dispersion of the Lamb wave in a PZT/metal/PZT sandwich plate considering the imperfect interface Seema and Singhal [21] investigated the transmission of SH waves in a magnetoelectroelastic solid cylindrical structure with different types of imperfect interfaces, using the spatially variable quasi-classical technique. Based on the generalized linear spring model (GLSM), effects of an imperfect interface on SH waves in various piezoelectric/piezomagnetic layered structures have been studied [22–24].

For the wave propagation problems in piezoelectric semiconductor structures, the existing research mainly focused on surface waves and bulk waves, while research on guided waves is still relatively limited [25–29]. Ben *et al.* [30] presented a numerical matrix solution to predict the dispersion curves of SH waves in a stressed piezoelectric semiconductor plate. By introducing the extended Stroh formalism, Tian *et al.* [31] derived the analytical formulation for elastic waves in an anisotropic PSC plate and investigated SH and Lamb waves in a ZnO PSC plate. Using the power series expansion method, Li *et al.* [32] investigated the influence of the surface effect, initial electron concentration, and plate thickness on the SH waves in a nanoplate based on the Gurtin–Murdoch surface model. Wei *et al.* [33] proposed an equivalent imperfect interface model of PN homojunction/ heterojunction of piezoelectric semiconductors and investigated the energy flux of the reflected and transmitted waves in multifields. Most of the above studies are about single-layered PSC plates or multilayered PSC plates with perfect interfaces. Studies on guided waves in multilayered plates considering the effect of an imperfect interface are few, which motivates the present study.

The primary contribution of this study lies in the application of an improved Legendre polynomial expansion method to model SH waves in multilayered PSC plates with considering interfacial imperfection. By integrating the Legendre polynomial approach with the imperfect interface conditions, the field variables associated with generalized displacements and tractions at the top and bottom interfaces of each layer are derived. The governing partial differential equations for the acoustic field are transformed into a generalized matrix eigenvalue problem in terms of the circular frequency ω, enabling the determination of the complete dispersion spectrum. Numerical examples are provided to demonstrate the influences of interface coefficients and stacking sequence on the phase velocity dispersion and attenuation behavior of SH waves in bilayered PSC plates composed of ZnO and GaN. These results provide valuable theoretical insights for controlling wave propagation in piezoelectric semiconductors and for the design of advanced acoustic devices.

2. Mathematical model of the problem

2.1. Basic formulation

Consider an n-type multilayered piezoelectric semiconductor plate with an imperfect interface, as shown in Fig 1. It should be noted that in p-type piezoelectric semiconductors, holes are the primary charge carriers, whereas in n-type piezoelectric semiconductors, free electrons are the primary charge carriers. Introducing a Cartesian coordinate system in such a way that the x-axis is in the direction of SH wave propagation, and the y-axis is in the polarization direction. Assuming N layers, each layer has a thickness of $h_1, h_2, \ldots, h_J$, and the total thickness of h, $h = h_1 + h_2 + \ldots + h_N$.

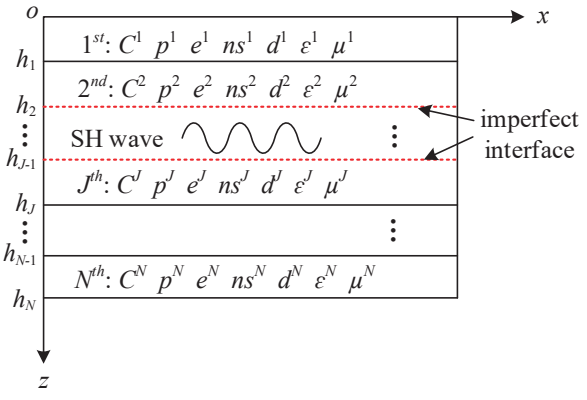

Fig. 1. Schematic diagram of a piezoelectric semiconductor multilayered plate.

The constitutive equations for a piezoelectric semiconductor structure are [26]:

$$\sigma_{ij} = c_{ijml}S_{ml} - e_{mij}E_m, \tag{2.1a}$$

$$D_i = e_{ikl}S_{kl} + \varepsilon_{ik}E_k, \tag{2.1b}$$

$$I_i = qn_s\mu_{ij}E_j + qn\mu_{ij}\bar{E}_P - qd_{ij}n_{,j}. \tag{2.1c}$$

The relationship between strain and displacement, as well as the relationship between electric field strength and potential, are:

$$S_{ij} = 0.5(u_{i,j} + u_{j,i}), \quad E_k = -\partial\varphi/\partial k. \tag{2.2}$$

The governing equations of a PSC structure consist of Newton's law, Gauss's law of electrostatics, and conservation of charge. In the absence of body forces and free charges, they are given [31],

$$\sigma_{ij,j} = \rho\ddot{u}_j, \quad D_{i,i} = qn, \quad q\dot{n} + I_{i,i} = 0 \tag{2.3}$$

in Eqs. (2.1)–(2.3), σ_{ij}, D_i, and I_i denote, respectively, stresses tensor, electric displacement vector, and electric current density vector. n_s denotes the steady state carrier concentration, c_{ijkl}, e_{kij}, ε_{ik}, μ_{ij}, and d_{ij} denote the elastic constant tensor, piezoelectric coefficient tensor, dielectric constant tensor, carrier mobility, and diffusion constant tensor, respectively. Here the Einstein summation convention is used, where $i, j, k, l, p = 1, 2, 3$, correspond to x, y, and z, respectively, with contracted subscripts (11→1, 22→2, 33→3, 23→4, 13→5, 12→6). n, φ, S_{kl}, E_k, and $\bar{E}_p$ represent the perturbation carrier concentration, electric potential, strain vector, electric field vector, and bias electric field vector, respectively; q is the elementary charge constant, and $q = 1.602 \times 10^{-19}$ C; "$,$" indicates the partial derivative of the corresponding coordinate, "." and ".." indicate the first-order and the second-order partial differentiations with respect to time t, respectively; the repeated index in the subscript represents the sum of the corresponding coordinates.

For traction-free and electrical open-circuit boundary conditions, we have [28],

$$\sigma_{zz} = \sigma_{zx} = \sigma_{zy} = 0, \quad D_z = 0, \quad I_z = 0, \quad \text{at } z = 0 \text{ and } z = h. \tag{2.4}$$

For the convenience of handling boundary conditions, a rectangular window function $\pi(z)$, is introduced:

$$\pi_{0,h_N}(z) = \begin{cases} 1, & 0 \le z \le h_N, \\ 0, & \text{else.} \end{cases} \tag{2.5}$$

For layered structures, the material parameters of the n-th can be expressed as [34]:

$$
\begin{aligned}
c_{ij} &= \sum_{n=1}^{N} c_{ij}^{(n)} \pi_{h_{n-1},h_n}(z), \quad e_{ij} = \sum_{n=1}^{N} e_{ij}^{(n)} \pi_{h_{n-1},h_n}(z), \\
\varepsilon_{ij} &= \sum_{n=1}^{N} \varepsilon_{ij}^{(n)} \pi_{h_{n-1},h_n}(z), \quad \mu_{ij} = \sum_{n=1}^{N} \mu_{ij}^{(n)} \pi_{h_{n-1},h_n}(z), \\
d_{ij} &= \sum_{n=1}^{N} d_{ij}^{(n)} \pi_{h_{n-1},h_n}(z).
\end{aligned} \tag{2.6}
$$

For the SH wave, the displacement, electric potential, and perturbation carrier concentration are assumed to be of the form:

$$
\{u_y, \varphi, n\}\{x, z, t\} = \{V(z), X(z), Y(z)\} \exp(\mathrm{i}kx - \mathrm{i}\omega t), \tag{2.7}
$$

where k and ω denote respectively the wavenumber and the angular frequency; i is the imaginary unit. $V(z)$, $X(z)$, and $Y(z)$ denote, respectively, amplitudes of the displacement, the electric potential, and the perturbation of the carrier density.

Substituting Eqs. (2.1), (2.2), (2.6), and (2.7) into Eq. (2.3) yields:

$$
\begin{aligned}
&(-c_{44}k^2V(z) - e_{15}k^2X(z) + c_{44}V''(z) + e_{15}X''(z))\pi(z) \\
&\qquad + \pi'(z)(c_{44}V'(z) + e_{15}X'(z)) = -\rho\omega^2 V(z),
\end{aligned} \tag{2.8a}
$$

$$
\begin{aligned}
&(-e_{15}k^2V(z) + \varepsilon_{11}k^2X(z) + e_{15}V''(z) - \varepsilon_{11}X''(z))\pi(z) \\
&\qquad + \pi'(z)(e_{15}V'(z) - \varepsilon_{11}X'(z)) = qY(z),
\end{aligned} \tag{2.8b}
$$

$$
\begin{aligned}
&(-\mu_{11}k^2n_sX(z) - d_{11}k^2Y(z) - \mathrm{i}\mu_{11}kE_1Y(z) + \mu_{11}n_sX''(z) \\
&\qquad + d_{11}Y''(z) - \mu_{11}E_3Y'(z))\pi(z) + \pi'(z)(\mu_{11}n_sX'(z) \\
&\qquad + d_{11}Y'(z) - \mu_{11}E_3Y(z)) = -\mathrm{i}\omega Y(z).
\end{aligned} \tag{2.8c}
$$

For the imperfect interface case, it is necessary to satisfy the generalized stress continuity (the stress, electric displacement, and electric current) and generalized displacement (the displacement, electric potential, and carrier density) discontinuity. Namely, at the imperfect interface $z = h_J$, the interface conditions are [35]:

$$
\sigma_{zy}^{(J)}(x, h_J) = \sigma_{zy}^{(J+1)}(x, h_J), \quad u_y^{(J+1)}(x, h_J) - u_y^{(J)}(x, h_J) = \alpha_1 \sigma_{zy}(x, h_J), \tag{2.9a}
$$

$$
D_z^{(J)}(x, h_J) = D_z^{(J+1)}(x, h_J), \quad \varphi^{(J+1)}(x, h_J) - \varphi^{(J)}(x, h_J) = -\alpha_2 D_z(x, h_J), \tag{2.9b}
$$

$$
I_z^{(J)}(x, h_J) = I_z^{(J+1)}(x, h_J), \quad n^{(J+1)}(x, h_J) - n^{(J)}(x, h_J) = -\alpha_3 I_z(x, h_J), \tag{2.9c}
$$

where α_1, α_2, and α_3 denote the interface parameters characterizing the interfacial imperfection related to mechanical displacement, electric displacement and potential, and carrier density, with units of m^3/N, Vm^2/C, and $\mathrm{s/mC}$, respectively. These parameters describe the degree of the interfacial bonding. When α_i is zero, the general interface is reduced to a perfect one. As increasing α_i, the bonding quality becomes poorer. When α_i approaches infinity, it indicates a complete stratification.

2.2. Solution of the problem

To satisfy the generalized displacement discontinuity conditions, the field quantities of each layer are expanded into individual Legendre polynomials. By combining these with Eq. (2.9), the imperfect interface model is incorporated into the Legendre polynomials associated with the imperfect interface layer. The field quantities of each layer can then be expressed as follows.

For the first layer:

$$\begin{aligned} V^{(1)}(z) &= \sum_{m=0}^{\infty} p_{m,1}^{(1)} Q_m^{(1)}(z), \qquad X^{(1)}(z) = \sum_{m=0}^{\infty} p_{m,2}^{(1)} Q_m^{(1)}(z), \\ Y^{(1)}(z) &= \sum_{m=0}^{\infty} p_{m,3}^{(1)} Q_m^{(1)}(z), \end{aligned} \tag{2.10a}$$

where $Q_m^{(1)}(z) = \sqrt{\frac{2m+1}{h_1}} P_m\big(\frac{2z}{h_1} - 1\big)$, with P_m being the m-th Legendre polynomial.

For the second layer:

$$\begin{aligned} V^{(2)}(z) &= V^{(1)}(h_1) + \alpha_1 c_{44}^{(1)} V^{(1)'}(z \to h_1) \\ &\quad + \alpha_1 e_{15}^{(1)} X^{(1)'}(z \to h_1) + (z - h_1) \sum_{m=0}^{\infty} p_{m,1}^{(2)} Q_m^{(2)}(z), \\ X^{(2)}(z) &= (z/h_1)^2 X^{(1)}(h_1) - \alpha_2 e_{15}^{(1)} V^{(1)'}(z \to h_1) \\ &\quad + \alpha_2 \varepsilon_{11}^{(1)} X^{(1)'}(z \to h_1) + (z - h_1) \sum_{m=0}^{\infty} p_{m,2}^{(2)} Q_m^{(2)}(z), \\ Y^2(z) &= (z/h_1)^2 Y^{(1)}(h_1) + q n_s \alpha_3 \mu_{11}^{(1)} X^{(1)'}(z \to h_J) \\ &\quad + q \alpha_3 d_{11}^{(1)} Y^{(1)'}(z \to h_J) + (z - h_1) \sum_{m=0}^{\infty} p_{m,3}^{(2)} Q_m^{(2)}(z), \end{aligned} \tag{2.10b}$$

where

$$Q_m^{(2)}(z) = \sqrt{\frac{2m+1}{h_2 - h_1}} P_m\left(\frac{2}{h_2 - h_1} z - \frac{h_2 + h_1}{h_2 - h_1}\right).$$

For layer $(J+1)$:

$$
\begin{aligned}
V^{(J+1)}(z) &= V^{(J)}(h_J) + \alpha_1 C_{44}^{(J)} V^{(J)'}(z \to h_J) \\
&\quad + \alpha_1 e_{15}^{(J)} X^{(J)'}(z \to h_J) + (z - h_J) \sum_{m=0}^{\infty} p_{m,1}^{(J+1)} Q_m^{(J+1)}(z), \\
X^{(J+1)}(z) &= (z/h_J)^2 X^{(J)}(h_J) - \alpha_2 e_{15}^{(J)} V^{(J)'}(z \to h_1) \\
&\quad + \alpha_2 \varepsilon_{11}^{(J)} X^{(J)'}(z \to h_1) + (z - h_J) \sum_{m=0}^{\infty} p_{m,2}^{(J+1)} Q_m^{(J+1)}(z), \\
Y^{(J+1)}(z) &= (z/h_J)^2 Y^{(J)}(h_J) + q n_s \alpha_3 \mu_{11}^{(J)} X^{(J)'}(z \to h_J) \\
&\quad + q \alpha_3 d_{11}^{(J)} Y^{(J)'}(z \to h_J) + (z - h_J) \sum_{m=0}^{\infty} p_{m,3}^{(J+1)} Q_m^{(J+1)}(z),
\end{aligned}
\tag{2.10c}
$$

where

$$
Q_m^{(J+1)}(z) = \sqrt{\frac{2m+1}{h_{J+1} - h_J}} P_m\left(\frac{2}{h_{J+1} - h_J} z - \frac{h_{J+1} + h_J}{h_{J+1} - h_J} \right),
$$

where $p_{m,n}^{(J)}$ denotes the undermined polynomial coefficients of the m-th Legendre polynomial of the n-th field quantity, and the superscript (J) represents the J-th layer. When m reaches a finite value M, the polynomial converges, and high-order terms can be ignored.

Substituting Eqs. (2.10) into Eqs. (2.8), multiplying both sides of the resulting equations by $Q_l^{(1)}(z)$, $Q_l^{(2)}(z)$, ..., $Q_l^{(N)}(z)$, with l from 0 to M, integrating over z from 0 to h_N, and using the orthonormality of the Legendre polynomial, and then rearranging the terms in the matrix equation so that the k dependence of the different terms becomes more apparent, leads to the following expression:

(2.11)

$$
\begin{aligned}
&k^2 \begin{bmatrix} {}^{(J)}A_{11}^{l,m} & {}^{(J)}A_{12}^{l,m} & {}^{(J)}A_{13}^{l,m} \\ {}^{(J)}A_{21}^{l,m} & {}^{(J)}A_{22}^{l,m} & {}^{(J)}A_{23}^{l,m} \\ {}^{(J)}A_{31}^{l,m} & {}^{(J)}A_{32}^{l,m} & {}^{(J)}A_{33}^{l,m} \end{bmatrix} \begin{bmatrix} p_{m,1}^{(J)} \\ p_{m,2}^{(J)} \\ p_{m,3}^{(J)} \end{bmatrix} + k \begin{bmatrix} {}^{(J)}B_{11}^{l,m} & {}^{(J)}B_{12}^{l,m} & {}^{(J)}B_{13}^{l,m} \\ {}^{(J)}B_{21}^{l,m} & {}^{(J)}B_{22}^{l,m} & {}^{(J)}B_{23}^{l,m} \\ {}^{(J)}B_{31}^{l,m} & {}^{(J)}B_{32}^{l,m} & {}^{(J)}B_{33}^{l,m} \end{bmatrix} \begin{bmatrix} p_{m,1}^{(J)} \\ p_{m,2}^{(J)} \\ p_{m,3}^{(J)} \end{bmatrix} \\
&+ \begin{bmatrix} {}^{(J)}C_{11}^{l,m} & {}^{(J)}C_{12}^{l,m} & {}^{(J)}C_{13}^{l,m} \\ {}^{(J)}C_{21}^{l,m} & {}^{(J)}C_{22}^{l,m} & {}^{(J)}C_{23}^{l,m} \\ {}^{(J)}C_{31}^{l,m} & {}^{(J)}C_{32}^{l,m} & {}^{(J)}C_{33}^{l,m} \end{bmatrix} \begin{bmatrix} p_{m,1}^{(J)} \\ p_{m,2}^{(J)} \\ p_{m,3}^{(J)} \end{bmatrix} = \begin{bmatrix} {}^{(J)}D_{11}^{l,m} & 0 & 0 \\ 0 & {}^{(J)}D_{22}^{l,m} & 0 \\ 0 & 0 & {}^{(J)}D_{33}^{l,m} \end{bmatrix} \begin{bmatrix} p_{m,1}^{(J)} \\ p_{m,2}^{(J)} \\ p_{m,3}^{(J)} \end{bmatrix}.
\end{aligned}
$$

Equation (2.11) can also be abbreviated as:

$$
k^2 \boldsymbol{AP} + k \boldsymbol{BP} + \boldsymbol{CP} = \boldsymbol{DP}, \tag{2.12}
$$

where $\boldsymbol{A}$, $\boldsymbol{B}$, $\boldsymbol{C}$, and $\boldsymbol{D}$ are all 3 $(M+1)$ order square matrices, and $\boldsymbol{P} = [p_{m,1}^{(J)}, p_{m,2}^{(J)}, p_{m,3}^{(J)}]^{\mathrm{T}}$. The non-zero elements in the matrix are given in the appendix.

It should be pointed out that k is purely real for elastic materials, therefore it is very efficient to solve the eigenvalues ω^2 by scanning specific k, as adopted in [36]. However, for piezoelectric semiconductor materials, k is complex, and the method is ineffective due to the presence of multivariate search. To deal with this problem, we develop a new solution procedure to transform the quadratic eigenvalue problem of Eq. (2.12) into a typical generalized eigenvalue problem in complex wavenumber k, based on a mathematical technique known as the Linear Companion Matrix Method.

Introducing a new vector $\boldsymbol{H}$, $\boldsymbol{H} = k \cdot \boldsymbol{P}$, and combining Eq. (2.12), gives

$$\begin{bmatrix} \boldsymbol{Z} & \boldsymbol{I} \\ \boldsymbol{A}^{-1}(\boldsymbol{D}-\boldsymbol{C}) & \boldsymbol{Z} \end{bmatrix} \cdot \boldsymbol{R} = k \cdot \boldsymbol{R}, \tag{2.13}$$

where $\boldsymbol{I}$ is the identity matrix, $\boldsymbol{Z}$ is a zero matrix. $\boldsymbol{R} = [\boldsymbol{P}\ \boldsymbol{H}]^{\mathrm{T}}$.

Consequently, the solution of Eq. (2.13) can obtain the complex wavenumber $k(\omega)$ eigenvalues and the field profile eigenvectors. Defining $k = \mathrm{Re}(k) + \mathrm{Im}(k)$, $\mathrm{Re}(k)$ and $\mathrm{Im}(k)$ denote respectively the real and imaginary parts of the wavenumber k, representing the propagation and attenuation of the wave. The phase velocity can be calculated by $V_{\mathrm{p}} = \omega/\mathrm{Re}(k)$. It should be clear that the calculation process involves different Legendre polynomials and their derivatives in each layer of the integration kernel function, resulting in a large number of numerical integration calculations, which are very time-consuming (sometimes several hours) to solve. To overcome these shortcomings, an analytical integration Legendre polynomial method is presented based on the orthogonal completeness and recursion of Legendre polynomials, which uses analytical integration instead of numerical integration to effectively reduce integration calculation time. There are five integral forms involved in calculations as follows:

$$\begin{aligned} I_1 &= \int_{-1}^{1} P_n(t) P_m(t)\, dt, \qquad I_2 = \int_{-1}^{1} P_n(t) \frac{d}{dt} P_m(t)\, dt, \\ I_3 &= \int_{-1}^{1} P_n(t) \frac{d^2}{dt^2} P_m(t)\, dt, \quad I_4 = \int_{-1}^{1} P_n(t) P_m(t) \frac{d}{dt}[h(t+1) - h(t-1)]\, dt, \\ I_5 &= \int_{-1}^{1} P_n(t) \frac{d}{dt} P_m(t) \frac{d}{dt}[h(t+1) - h(t-1)]\, dt. \end{aligned} \tag{2.14}$$

Based on the completeness and recursion of Legendre polynomials, the analytical expression is derived as follows:

$$I_1 = \begin{cases} \displaystyle\sum_{s=0}^{\lfloor m/2 \rfloor} (-1)^s \frac{(2m-2s)!}{2^m s!(m-s)!(m-2s)!} \frac{2^{n+1}(n+2p)!(n+p)!}{p!(2n+2p+1)!}, \\ \qquad m > n,\ \mathrm{mod}(m-n,2) = 0,\ m-2s = n+2p, \\ 0, \qquad \text{else}, \end{cases} \tag{2.15}$$

$$I_2 = \begin{cases} \displaystyle\sum_{s=0}^{\lfloor m/2 \rfloor} (-1)^s \frac{(2m-2s)!}{2^m s!(m-s)!(m-2s)!} \frac{2^{n+1}(n+2p)!(n+p)!}{p!(2n+2p)!}, \\ \qquad m-1 \geq n,\ \mathrm{mod}(m-n-1,2) = 0,\ m-2s-1 = n+2p, \\ 0, \qquad \text{else}, \end{cases} \tag{2.16}$$

$$I_3 = \begin{cases} \displaystyle\sum_{s=0}^{\lfloor m/2 \rfloor} (-1)^s \frac{(2m-2s)!}{2^m s!(m-s)!(m-2s)!} \frac{2^{n+1}(n+2p)!(n+p)!}{p!(2n+2p-1)!}, \\ \qquad m-2 \geq n,\ \mathrm{mod}(m-n-2,2) = 0,\ m-2s-2 = n+2p, \\ 0, \qquad \text{else}. \end{cases} \tag{2.17}$$

By utilizing the properties of the Heaviside function $h(t)$, I_4 and I_5 can be obtained:

$$I_4 = P_n(-1)P_m(-1) - P_n(1)P_m(1), \tag{2.18}$$

$$I_5 = P_n(-1)\left[\frac{d}{dt}P_m(t)\right]_{t=-1} - P_n(1)\left[\frac{d}{dt}P_m(t)\right]_{t=1}. \tag{2.19}$$

3. Numerical results and discussion

Based on the above derivation, a computer program in terms of the Legendre polynomial has been written to calculate the dispersion of SH waves in ZnO/GaN piezoelectric semiconductor multilayered plates with imperfect interfaces. The material parameters from [31, 37] are given in Table 1.

3.1. Verification of the method

To verify the correctness of the presented method, we first calculate the phase velocity dispersion curves of the SH wave in a twolayered PSC plate with interface coefficients of 0, i.e., degenerating into an ideal interface. Since both the upper and lower layers are ZnO, this structure is equivalent to a single-layer ZnO plate. The dimensionless wavenumber is defined as kh and the phase velocity

TABLE 1. Material parameters.

Materials	c_{11}	c_{13}	c_{33}	c_{44}	e_{15}	e_{31}	e_{33}
ZnO	210	105	211	43	−0.48	−0.57	1.32
GaN	379	107	380	98	−0.33	−0.46	0.77
Materials	ε_{11}	ε_{33}	μ_{11}	μ_{33}	d_{11}	d_{33}	ρ
ZnO	7.61	8.85	1	1	0.026	0.026	5700
GaN	8.41	9.12	6.53	9.82	0.1699	0.2553	6095

Units: c_{ij} [GPa], e_{ij} [C/m^2], ε_{ij} [$\times 10^{-11}$ F/m], μ_{ij} [m^2/V], d_{ij} [m^2/s], ρ [kg/m^3].

$\mathrm{Re}(c) = \omega/\mathrm{Re}(k)$, respectively. The thicknesses of the upper and lower layers are equal, the total thickness h is set to 1 mm, 2 mm, 3 mm, and 4 mm, respectively; n_s is taken as 2×10^{15} m^{-3}, and M is set to 16. The material parameters are listed in Table 1. Figure 2 shows the phase velocity dispersion curves obtained using the improved Legendre orthogonal polynomial method. Its excellent agreement with those shown in the original paper by TIAN *et al.* [31] was checked by the authors and no difference was found between the two sets. Therefore, the results from Tian *et al.* are not reproduced here but can be found in [31]. This confirms the accuracy and reliability of the proposed method.

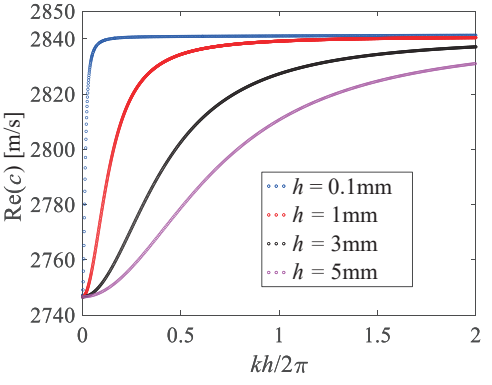

FIG. 2. Phase velocity dispersion curves of SH wave in ZnO plates.

3.2. SH waves in a ZnO plate

The presented method can calculate the complete three-dimensional (3D) spectrum. The three-dimensional spectrum of the SH wave, as well as the two-dimensional dispersion and attenuation curves, are calculated for a ZnO plate with $h = 3$ mm, $n_s = 10^{15}$ m^{-3}, as depicted in Figs. 3a and 3b. The dimensionless frequency is $\Omega = \omega h\sqrt{c_{11}/\rho}$. For comparison purposes, only the first

several modes are plotted Figs. 3c and 3d are the dispersion and attenuation curves for $n_s = 10^{15}$ m^{-3}. It can be observed from Figs. 3c and 3d that each of these modes has no cutoff frequency and can propagate in the whole frequency domain, which is different from the piezoelectric and pure elastic plates. But for $n_s = 10^{26}$ m^{-3}, the SH1 mode has a cutoff frequency (as marked by the circle in Fig. 3a), indicating that the modulation of wave characteristics can be achieved by changing n_s.

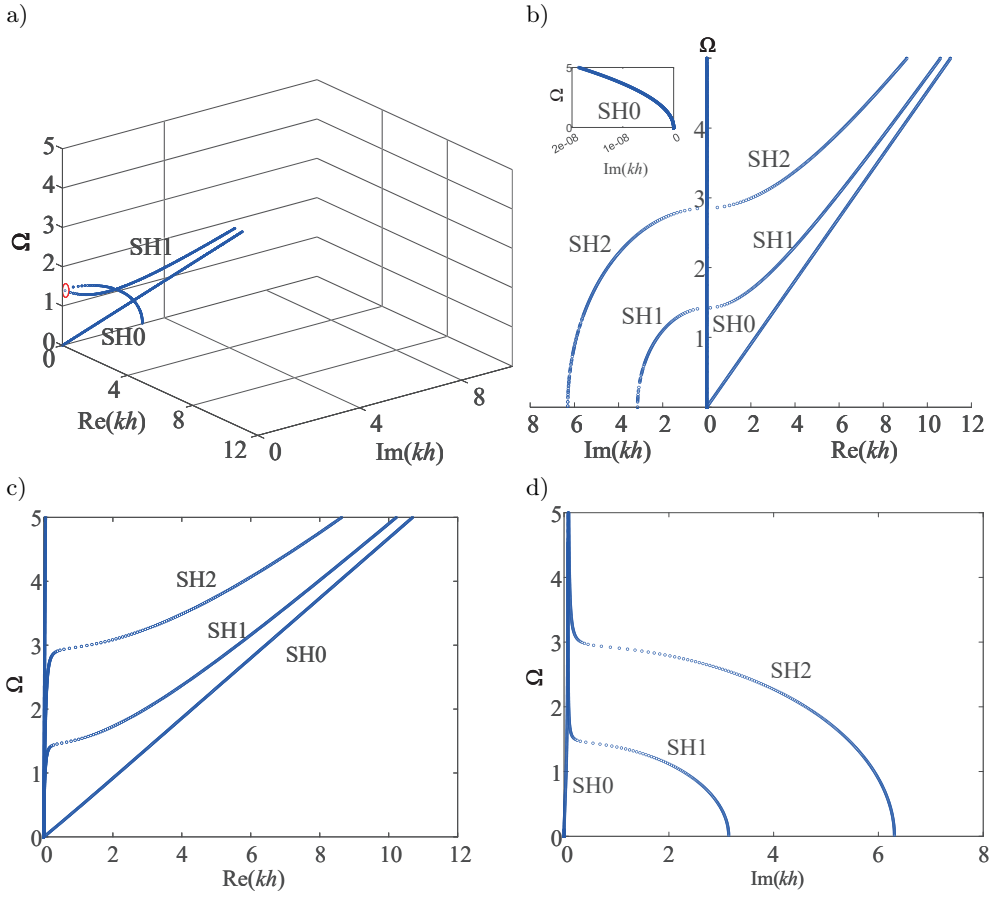

Fig. 3. SH waves in ZnO plates with different n_s: a) and b) are the 3D and 2D spectrum for $n_s = 10^{26}$ m^{-3}, and c) and d) are the dispersion and attenuation for $n_s = 10^{15}$ m^{-3}.

Further calculations are conducted on k for different n_s at $\Omega = 5$, and the relationships between n_s and Re(kh), n_s and Im(kh) are obtained, as depicted in Fig. 4. When n_s is less than the critical value of $10^{14.5}$ m^{-3} or greater than $10^{16.5}$ m^{-3}, k tends towards a constant value; that is, the wave speed no longer changes. The attenuation is also very small. For a ZnO piezoelec-

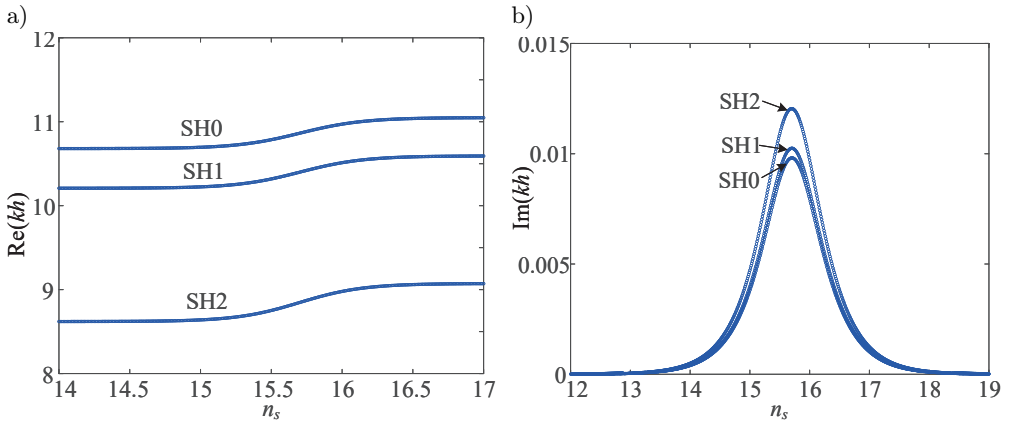

FIG. 4. The relationship curves when $\Omega = 5$, a) n_s vs Re(kh), b) n_s vs Im(kh).

tric plate (q, μ_{ij} and d_{ij} are 0), the phase velocity of SH0 mode calculated by $V_p = \sqrt{c_{44} + e_{15}^2/\varepsilon_{11}/\rho}$ is 2841.66 m/s. For a ZnO elastic plate (q, e_{ij}, ε_{ij}, μ_{ij}, and d_{ij} are 0) the corresponding phase velocity is 2746.61 m/s. The resulting phase velocities of the SH0 mode for ZnO PSC plates with different n_s, $n_s = 10^{26}$ m^{-3} and $n_s = 10^6$ m^{-3}, are respectively 2841.66 m/s and 2746.61 m/s, as shown in Fig. 5. This indicates that when n_s is below a certain critical value, the PSC plate behaves like a piezoelectric plate, devoid of the semiconductor effect. When n_s exceeds a certain critical value, the PSC plate behaves like an elastic plate, free of both piezoelectric and semiconductor effects. Therefore, when designing PSC structures with larger wave amplitudes, it is necessary to determine n_s and avoid the critical value.

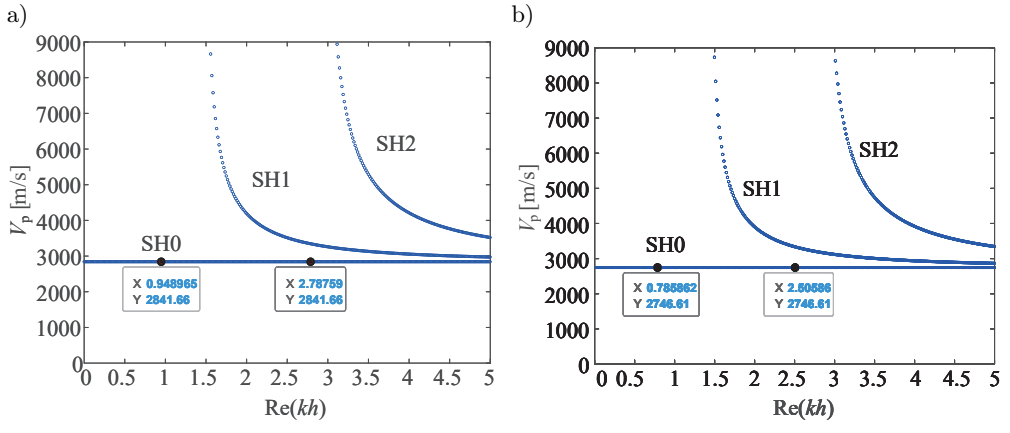

FIG. 5. Phase velocity curves for different n_s, a) $n_s = 10^{26}$ m^{-3}, b) $n_s = 10^6$ m^{-3}.

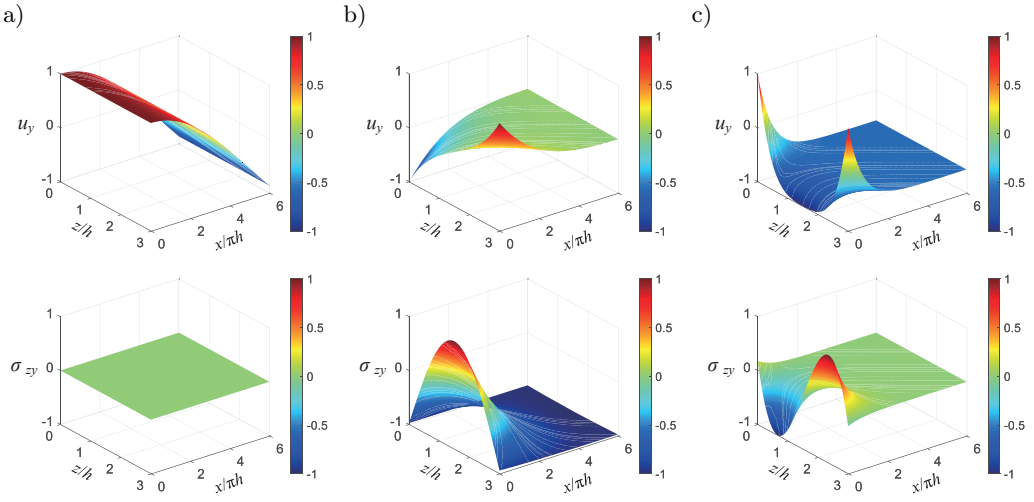

Fig. 6. Distributions of displacement and stress, at $\mathrm{Re}(kh) = 0.3$, a) SH0 mode, b) SH1 mode, and c) SH2 mode.

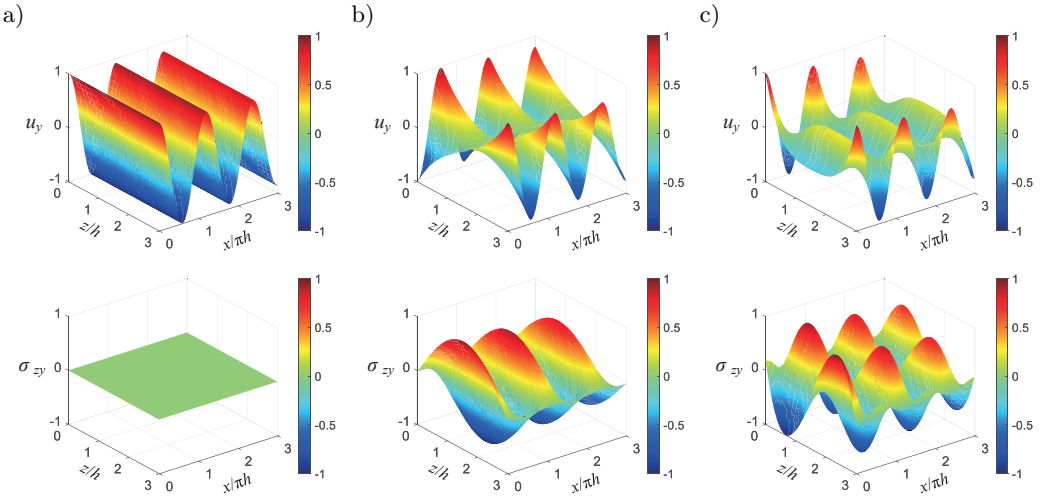

Fig. 7. Distributions of displacement and stress, at $\mathrm{Re}(kh) = 5$, a) SH0 mode, b) SH1 mode, c) SH2 mode.

In addition, the distributions of displacement and stress at specific wavenumbers are analyzed to illustrate the wave propagation characteristics of SH waves. They can be easily obtained by substituting the eigenvectors into Eqs. (2.7) with the Legendre polynomial. Figures 6 and 7 respectively show the normalized displacement u_y and the normalized stress σ_{zy} along the thickness direction and wave propagation direction for the first three modes at $\mathrm{Re}(kh) = 0.3$ and

$\mathrm{Re}(kh) = 5$. As seen in Figs. 6 and 7, for the SH0 mode, u_y remains constant along the thickness direction, and σ_{zy} is zero. For the SH1 and SH2 modes, the distributions of the displacement and stress are antisymmetric and symmetric, respectively. The attenuation of SH waves is more significant at $\mathrm{Re}(kh) = 0.3$ than at $\mathrm{Re}(kh) = 5$, which is due to the larger ratio of $\mathrm{Im}(kh)/\mathrm{Re}(kh)$ in the former case. Additionally, the stress on the top and bottom surfaces is zero, consistent with the preset free boundary conditions. This further confirms the correctness of the method.

3.3. Effect of the imperfect interface on SH waves in ZnO/GaN bilayered plates

To illustrate the effect of different interface coefficients on SH waves, the wavenumbers of the first three modes at $\Omega = 5$ for a ZnO/GaN bilayered plate with $h_1 = h_2 = 1.5$ mm, $n_s = 10^{16}$ m^{-3}, $\bar{E}_1 = 10^4$ N/C, and $\bar{E}_3 = 0$ are calculated, as listed in Table 2. The dimensionless interface parameters are $\gamma_1 = c_{11}\alpha_1/h$, $\gamma_2 = -\varepsilon_{11}\alpha_2/h$, and $\gamma_3 = -d_{11}\alpha_3/h$. From Table 2, we can observe that the effect of γ_1 is significant, the effect of γ_2 is small, and γ_3 has almost no effect. As γ_1 increases, $\mathrm{Re}(kh)$ of the first three modes increases. The subsequent research will mainly focus on the effect of γ_1.

TABLE 2. The wavenumbers of the first three modes at $\Omega = 5$.

Interface coefficients		SH0		SH1		SH2	
		$\mathrm{Re}(kh)$	$\mathrm{Im}(kh)$	$\mathrm{Re}(kh)$	$\mathrm{Im}(kh)$	$\mathrm{Re}(kh)$	$\mathrm{Im}(kh)$
γ_1 ($\gamma_2 = \gamma_3 = 0$)	0	10.3102	0.0722	6.3729	0.0571	7.8525	0.0628
	1	10.4677	0.0723	7.1703	0.0871	8.079	0.0329
	10	10.6546	0.0725	7.4846	0.0926	8.5773	0.0208
γ_2 ($\gamma_1 = \gamma_3 = 0$)	0	10.3102	0.0722	6.3729	0.0571	7.8525	0.0628
	1	10.3088	0.0721	6.3694	0.0500	7.8406	0.0661
	10	10.3091	0.0721	6.3702	0.0508	7.8428	0.0646
γ_3 ($\gamma_1 = \gamma_2 = 0$)	0	10.3102	0.0722	6.3729	0.0571	7.8525	0.0628
	1	10.3102	0.0722	6.3729	0.0571	7.8525	0.0628
	10	10.3102	0.0722	6.3729	0.0571	7.8525	0.0628

Figure 8 illustrates the dispersion and attenuation of the first three modes of ZnO/GaN bilayered plates with varying $\gamma_1(\gamma_2 = \gamma_3 = 0)$. It can be noticed that the effect of γ_1 on different modes varies. $\mathrm{Re}(kh)$ for each mode increases with increasing γ_1. The impact of γ_1 on the SH0 mode is relatively small and regular, whereas its effect on the SH1 and SH2 modes is significant. For example, the $\mathrm{Re}(kh)$ for the SH2 mode is 0.24, 2.44, and 3.98 at $\Omega = 3.5$, for γ_1 values of 0, 1, and 10 respectively. The $\mathrm{Im}(kh)$ for the SH1 mode decreases markedly with increasing γ_1. For example, the $\mathrm{Im}(kh)$ for the SH1 mode is 2.98, 2.26 and

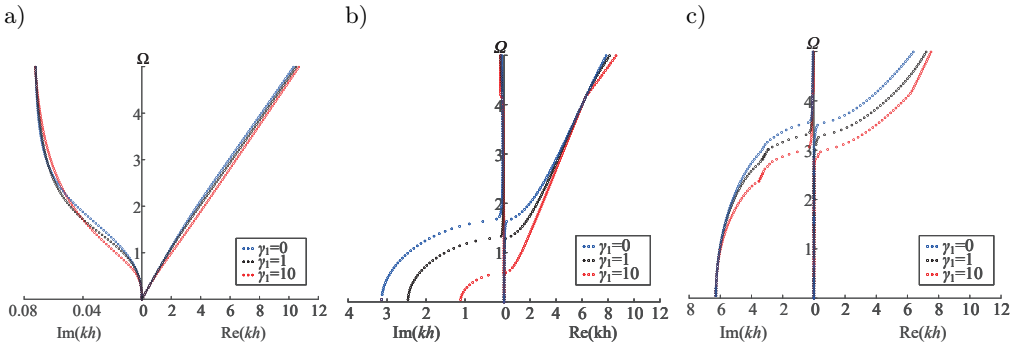

Fig. 8. The influence of γ_1 on dispersion, a) SH0 mode, b) SH1 mode, c) SH2 mode.

0.58 at $\Omega = 0.5$, for γ_1 values of 0, 1, and 10, respectively. In contrast to the SH1 mode, the influence of γ_1 on the Im(kh) of the SH2 mode is minimal in the low-frequency region but becomes increasingly significant as the frequency increases. This behavior differs from its effect on the SH1 mode.

Figure 9 displays the phase velocity of the first three SH wave modes for various values of γ_1. It can be observed that the phase velocity decreases as γ_1 increases. For example, when Re(kh) = 3 and γ_1 takes 0, 1, and 10, the phase velocities of the SH0 mode are 3308 m/s, 3191 m/s, and 2899 m/s, respectively, and those of the SH1 mode are 4819 m/s, 4494 m/s, and 4103 m/s, respectively.

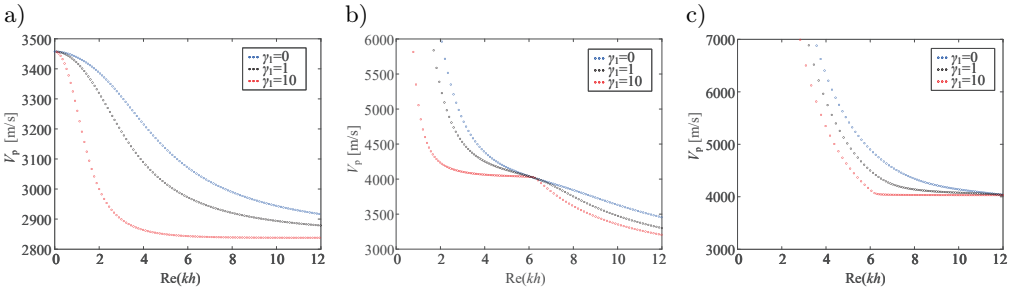

Fig. 9. The influence of γ_1 on phase velocity, a) SH0 mode, b) SH1 mode, c) SH2 mode.

3.4. SH waves in sandwich PSC plates with imperfect interfaces

Furthermore, the SH wave in PSC sandwich plates composed of ZnO and GaN with imperfect interfaces is investigated. The influence of γ_1 and stacking sequence on dispersion curves is illustrated. For convenience, ZnO and GaN are respectively represented by the letters Z and G. Consider two types of sandwich plates, Z/G/Z and G/Z/G, with $h_1 = h_2 = h_3 = 1$ mm, $n_s = 10^{16}$ m^{-3}; γ_{11} and γ_{12} represent the interface coefficients between the first and second layers,

as well as between the second and third layers, respectively. Three interface cases are considered: (1) $\gamma_{11} = 1$, $\gamma_{12} = 3$, (2) $\gamma_{11} = \gamma_{12} = 2$, (3) $\gamma_{11} = 3$, $\gamma_{12} = 1$.

Figure 10 presents the dispersion and attenuation curves for Z/G/Z sandwich plates with different interface coefficients, while Fig. 11 shows the corresponding phase velocity curves. From Figs. 10 and 11, it is evident that the interface coefficients have a relatively small effect on the SH0 mode, but a significant influence on the SH1 and SH2 modes. The SH1 mode exhibits the highest $\mathrm{Im}(kh)$, and thus the maximum attenuation, in case (3), and the lowest $\mathrm{Im}(kh)$ in case (1). In contrast, the SH2 mode shows the smallest $\mathrm{Im}(kh)$ in case (3) and the largest in case (1). The impact of the interface coefficients on the SH0 and SH2 modes is similar, with the phase velocity in case (1) being higher than that in case (3). However, for the SH1 mode, the pattern is reversed, as its phase velocity in case (1) is lower than in case (3). For instance, when $\mathrm{Re}(kh) = 2.5$, the phase velocities in the three cases are 3887 m/s, 4127 m/s, and 4480 m/s, respectively. Additionally, the influence of the interface coefficient decreases with increasing wavenumber.

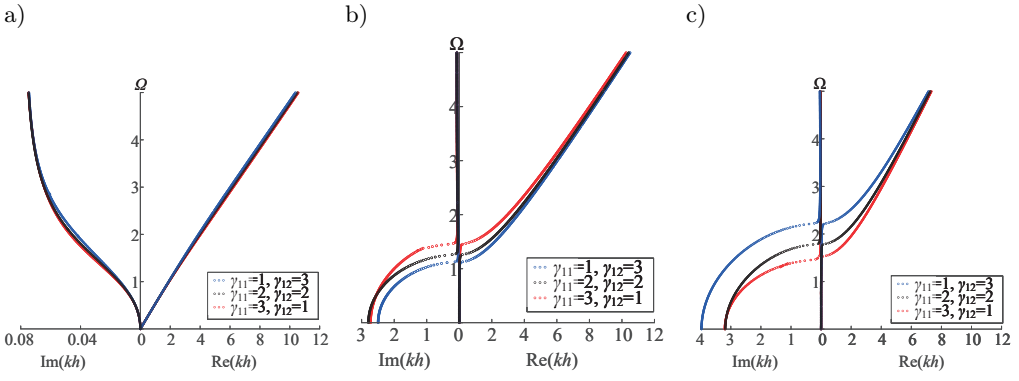

FIG. 10. Dispersion curves for Z/G/Z sandwich plates with different interface coefficients, a) SH0 mode, b) SH1 mode, c) SH2 mode.

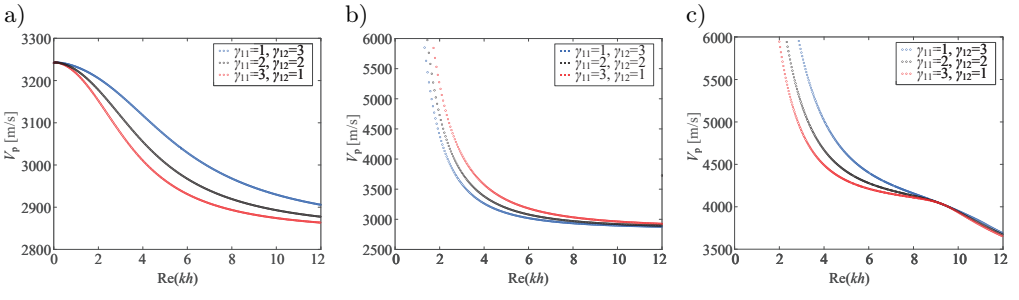

FIG. 11. Phase velocity for Z/G/Z sandwich plates with different interface coefficients, a) SH0 mode, b) SH1 mode, c) SH2 mode.

To illustrate the effect of stacking sequence on SH waves, three types of sandwich plates, G/Z/Z, Z/G/Z, and Z/Z/G, are considered, with $\gamma_{11} = \gamma_{12} = 1$ and all other parameters remaining as previously described. Figure 12 shows the dispersion and attenuation curves of the first three modes of SH wave in these three sandwich plates, while Fig. 13 shows the corresponding phase velocity curves. Despite having the same material volume content, the dispersion and attenuation curves vary significantly among the three cases, indicating that the stacking sequence plays a crucial role in the behavior of SH waves. For the SH0 and SH2 modes, Re(kh) for the G/Z/Z plate is notably greater than that for the other two plates, which corresponds to a lower phase velocity. The difference in Re(kh) for the SH0 mode between the Z/G/Z and Z/Z/G plates is relatively small. For the SH0 mode, the difference in Im(kh) becomes more pronounced with increasing frequency in the three cases. At a specified frequency, the Z/G/Z plate exhibits the smallest Im(kh), whereas the G/Z/Z plate shows the largest. For the SH1 mode, the difference in Re(kh) between the Z/G/Z and Z/Z/G plates is relatively small and their phase velocities are very close, whereas the Re(kh) for the G/Z/Z plate is significantly greater. The difference between them becomes more pronounced with the increase of wavenumber. Unlike the SH0 and SH2

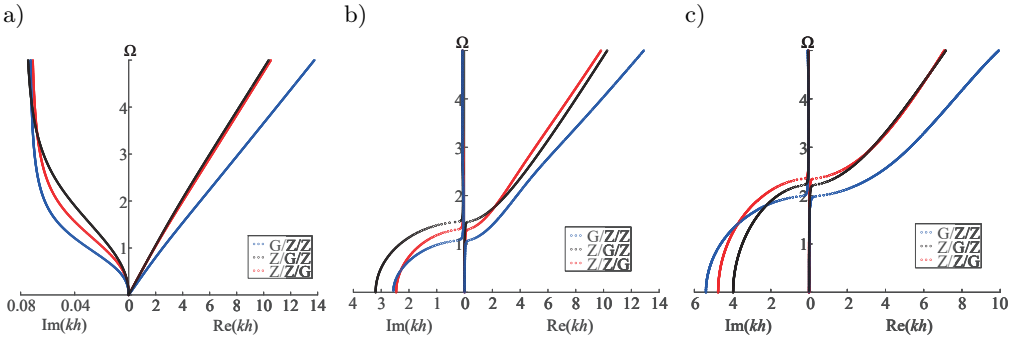

Fig. 12. Dispersion and attenuation for different sandwich plates, a) SH0 mode, b) SH1 mode, c) SH2 mode.

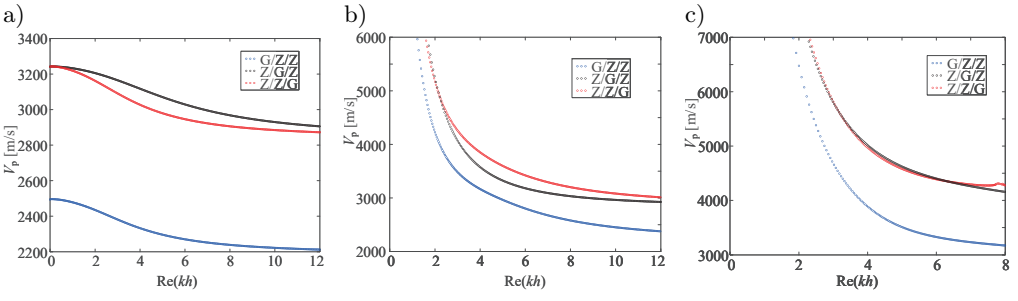

Fig. 13. Phase velocity for different sandwich plates, a) SH0 mode, b) SH1 mode, c) SH2 mode.

modes, the Im(kh) for the SH1 mode in the Z/G/Z plate is the biggest among the three cases, indicating a greater degree of attenuation compared to the other two plates.

4. Conclusions

The characteristics of SH waves in PSC multilayered plates with imperfect interfaces are investigated using an improved Legendre orthogonal polynomial method with analytical integration. Numerical computations and graphical exhibitions are carried out to show the influences of different interface coefficients and stacking sequences on SH waves in multilayered plates composed of the ZnO and GaN. Numerical results demonstrate the following conclusions:

(1) Based on the generalized linear spring model, the dispersion and attenuation of the SH waves in PSC multilayered plates with imperfect interfaces are derived using the improved Legendre orthogonal polynomial method. This method can avoid the tedious iterative search procedure to obtain complete solutions of the dispersion equation.

(2) When the steady-state carrier concentration n_s is below a certain critical value, the behavior of the SH wave in a PSC plate resembles that in a piezoelectric plate. Conversely, when n_s exceeds a certain critical value, the behavior tends to resemble that of an elastic plate. Adjusting n_s allows control of the wave behavior, making it a key parameter in the design of piezoelectric semiconductor devices.

(3) The interface coefficient γ_1 has the greatest impact on the SH wave, while γ_2 has a relatively small effect, and γ_3 has almost no effect. Re(kh) for each mode increases with the increase of γ_1, that is, the phase velocity decreases. The influence of γ_1 becomes more pronounced as the mode order increases.

(4) The stacking sequence significantly affects the SH waves. For SH0 and SH2 modes, the G/Z/Z plate has a lower phase velocity and higher attenuation than Z/G/Z and Z/Z/G plates. For SH1 mode, its phase velocity is also the smallest. By optimizing the layering sequence, the attenuation of waves in the material can be reduced, thereby improving the electromechanical conversion efficiency.

Future research could be extended to consider multi-physics fields involving temperature, as well as more complex structural configurations such as multilayered cylindrical structures and sector-shaped cross-section structures.

Appendix

$$A_{11}^{l,m} = -\sum_{J=0}^{N} c_{44}^{(J)} \int_{0}^{h} Q_l^{(J)}(z) Q_m^{(J)}(z)\, dz,$$

$$A_{12}^{l,m} = -\sum_{J=0}^{N} e_{15}^{(J)} \int_0^h Q_l^{(J)}(z) Q_m^{(J)}(z)\, dz,$$

$$A_{21}^{l,m} = -\sum_{J=0}^{N} e_{15}^{(J)} \int_0^h Q_l^{(J)}(z) Q_m^{(J)}(z)\, dz,$$

$$A_{22}^{l,m} = \sum_{J=0}^{N} \varepsilon_{11}^{(J)} \int_0^h Q_l^{(J)}(z) Q_m^{(J)}(z) dz,$$

$$A_{32}^{l,m} = -n_s \sum_{J=0}^{N} \mu_{11}^{(J)} \int_0^h Q_l^{(J)}(z) Q_m^{(J)}(z)\, dz,$$

$$A_{33}^{l,m} = -\sum_{J=0}^{N} d_{11}^{(J)} \int_0^h Q_l^{(J)}(z) Q_m^{(J)}(z)\, dz,$$

$$\begin{aligned} C_{11}^{l,m} = {} & \sum_{J=0}^{N} c_{44}^{(J)} \int_0^h Q_l^{(J)}(z) \frac{d^2}{dz^2} Q_m^{(J)}(z)\, dz \\ & + \sum_{J=0}^{N} c_{44}^{(J)} \int_0^h Q_l^{(J)}(z) \frac{d}{dz} Q_m^{(J)}(z) \frac{d\pi(z)}{dz}\, dz, \end{aligned}$$

$$\begin{aligned} C_{12}^{l,m} = {} & \sum_{J=0}^{N} e_{15}^{(J)} \int_0^h Q_l^{(J)}(z) \frac{d^2}{dz^2} Q_m^{(J)}(z)\, dz \\ & + \sum_{J=0}^{N} e_{15}^{(J)} \int_0^h Q_l^{(J)}(z) \frac{d}{dz} Q_m^{(J)}(z) \frac{d\pi(z)}{dz}\, dz, \end{aligned}$$

$$\begin{aligned} C_{21}^{l,m} = {} & \sum_{J=0}^{N} e_{15}^{(J)} \int_0^h Q_l^{(J)}(z) \frac{d^2}{dz^2} Q_m^{(J)}(z)\, dz \\ & + \sum_{J=0}^{N} e_{15}^{(J)} \int_0^h Q_l^{(J)}(z) \frac{d}{dz} Q_m^{(J)}(z) \frac{d\pi(z)}{dz}\, dz, \end{aligned}$$

$$\begin{aligned} C_{22}^{l,m} = {} & -\sum_{J=0}^{N} \varepsilon_{11}^{(J)} \int_0^h Q_l^{(J)}(z) \frac{d^2}{dz^2} Q_m^{(J)}(z)\, dz \\ & - \sum_{l=0}^{N} \varepsilon_{11}^{(J)} \int_0^h Q_l^{(J)}(z) \frac{d}{dz} Q_m^{(J)}(z) \frac{d\pi(z)}{dz}\, dz, \end{aligned}$$

$$C_{23}^{l,m} = -q \sum_{J=0}^{N} \int_0^h Q_l^{(J)}(z) Q_m^{(J)}(z)\, dz,$$

$$C_{32}^{l,m} = n_s \sum_{J=0}^{N} \mu_{11}^{(J)} \int_0^h Q_l^{(J)}(z) \frac{d^2}{dz^2} Q_m^{(J)}(z)\, dz + n_s \sum_{J=0}^{N} \mu_{11}^{(J)} \int_0^h Q_l^{(J)}(z) \frac{d}{dz} Q_m^{(J)}(z) \frac{d\pi(z)}{dz}\, dz,$$

$$C_{33}^{l,m} = \sum_{J=0}^{N} d_{11}^{(J)} \int_0^h Q_l^{(J)}(z) \frac{d^2}{dz^2} Q_m^{(J)}(z)\, dz + \sum_{J=0}^{N} d_{11}^{(J)} \int_0^h Q_l^{(J)}(z) \frac{d}{dz} Q_m^{(J)}(z) \frac{d\pi(z)}{dz}\, dz,$$

$$D_{11}^{l,m} = -\rho\omega^2 \sum_{J=0}^{N} \int_0^h Q_l^{(J)}(z) Q_m^{(J)}(z)\, dz,$$

$$D_{33}^{l,m} = -\mathrm{i}\omega \sum_{J=0}^{N} \int_0^h Q_l^{(J)}(z) Q_m^{(J)}(z)\, dz.$$

Disclosure statement

No potential conflict of interest was reported by the authors.

Acknowledgements

The work was supported by the National Natural Science Foundation of China (No. 12102131), the Fundamental Research Funds for the Universities of Henan Province (No. NSFRF240331), the innovative research team of Henan Polytechnic University (No. T2022-4), the Henan Polytechnic University double first-class discipline creation project (No. AQ20250712 and AQ20250710), and the Henan University Science and Technology Innovation Team Support Plan (No. 23IRTSTHN016).

References

1. G. Wang, J. Liu, X. Liu, W. Feng, J. Yang, *Extensional vibration characteristics and screening of polarization charges in a ZnO piezoelectric semiconductor nanofiber*, Journal of Applied Physics, **124**, 9, 094502, 2018.

2. J. Guo, G. Nie, J. Liu, L. Zhang, *Free vibration of a bi-layered composite plate of a piezoelectric semiconductor and a piezoelectric dielectric*, AIP Advances, **13**, 9, 095317, 2023.

3. A. Singhal, S.A. Sahu, S. Chaudhary, *Liouville-Green approximation: An analytical approach to study the elastic waves vibrations in composite structure of piezo material*, Composite Structures, **184**, 714–727, 2018.

4. A. Seema, A. Singhal, *Study of surface wave velocity in distinct rheological models with flexoelectric effect in piezoelectric aluminium nitride structure*, Journal of the Brazilian Society of Mechanical Sciences and Engineering, **47**, 1, 29, 2025.

5. D.L. Xiao, Q. Han, T. Jiang, *Guided wave propagation in a multilayered magneto-electro-elastic curved panel by Chebyshev spectral elements method*, Composite Structures, **207**, 701–710, 2019.

6. Q. Gao, Y. Zhang, *An accurate method for guided wave propagation in multilayered anisotropic piezoelectric structures*, Acta Mechanica, **231**, 5, 1783–1804, 2020.

7. J. Chen, E. Pan, H. Chen, *Wave propagation in magneto-electro-elastic multilayered plates*, International Journal of Solids and Structures, **44**, 34, 1073–1085, 2007.

8. H. Ezzin, M. Ben Amor, M.H. Ben Ghozlen, *Lamb waves propagation in layered piezoelectric/piezomagnetic plates*, Ultrasonics, **76**, 63–69, 2017.

9. J.S. Yang, X.M. Yang, J.A. Turner, *Amplification of acoustic waves in laminated piezoelectric semiconductor plates*, Archive of Applied Mechanics, **74**, 34, 288–298, 2004.

10. S. Gupta, N. Bhengra, *Implementation of finite difference approximation on the SH-wave propagation in a multilayered magnetoelastic orthotropic composite medium*, Acta Mechanica, **228**, 10, 3421–3444, 2017.

11. O. Matar, N. Gasmi, H. Zhou, M. Goueygou, A. Talbi, *Legendre and Laguerre polynomial approach for modeling of wave propagation in layered magneto-electro-elastic media*, Journal of the Acoustical Society of America, **133**, 3, 1415–1424, 2013.

12. C. Othmani, F. Takali, A. Njeh, *Modeling of phase velocity and frequency spectrum of guided Lamb waves in piezoelectric-semiconductor multilayered structures made of AlAs and GaAs*, Superlattices and Microstructures, **111**, 396–404, 2017.

13. C. Othmani, F. Takali, A. Njeh, *Theoretical study on the dispersion curves of Lamb waves in piezoelectric-semiconductor sandwich plates GaAs-FGPM-AlAs: Legendre polynomial series expansion*, Superlattices and Microstructures, **106**, 86–101, 2017.

14. M.X. Deng, *Analysis of second-harmonic generation of Lamb waves propagating in layered planar structures with imperfect interfaces*, Applied Physics Letters, **88**, 22, 221902, 2006.

15. X. Guo, P.J. Wei, *Effects of initial stress on the reflection and transmission waves at the interface between two piezoelectric half spaces*, International Journal of Solids and Structures, **51**, 21, 3735–3751, 2014.

16. T. Kepceler, *Torsional wave dispersion relations in a pre-stressed bi-material compounded cylinder with an imperfect interface*, Applied Mathematical Modelling, **34**, 12, 4058–4073, 2010.

17. G. Nie, J. Liu, X. Fang, Z. An, *Shear horizontal (SH) waves propagating in piezo-electricpiezomagnetic bilayer system with an imperfect interface*, Acta Mechanica, **223**, 9, 1999–2009, 2012.

18. G. NIE, J. LIU, X. LIU, *Lamb wave propagation in a piezoelectric/piezomagnetic bimaterial plate with an imperfect interface*, Acta Acustica United with Acustica, **102**, 5, 893–901, 2016.

19. S. CHAUDHARY, S.A. SAHU, A. SINGHAL, S. NIRWAL, *Interfacial imperfection study in pres-stressed rotating multiferroic cylindrical tube with wave vibration analytical approach*, Materials Research Express, **6**, 10, 105704, 2019.

20. I. KURT, S. AKBAROV, S. SEZER, *Lamb wave dispersion in a PZT/metal/PZT sandwich plate with imperfect interface*, Waves in Random and Complex Media, **26**, 3, 301–327, 2016.

21. A. SEEMA, A. SINGHAL, *Theoretical investigation of SH wave transmission in magneto-electro-elastic structure having imperfect interface using approximating method*, Applied Physics A, **130**, 8, 597, 2024.

22. H. KUO, S. YU, *Effect of the imperfect interface on the scattering of SH wave in a piezoelectric cylinder in a piezomagnetic matrix*, International Journal of Engineering Science, **85**, 186–202, 2014.

23. S. KUMARI, S. SAHU, K. PANKAJ, *Analysis of SH wave in hollow piezo-composite cylinder with coupled imperfect interface condition*, Mechanics Based Design of Structures and Machines, **51**, 4, 2080–2100, 2023.

24. P. KUMAR, M. MAHANTY, A. CHATTOPADHYAY, A. SINGH, *Effect of interfacial imperfection on shear wave propagation in a piezoelectric composite structure: Wentzel–Kramers–Brillouin asymptotic approach*, Journal of Intelligent Material Systems and Structures, **30**, 1819, 2789–2807, 2019.

25. J.N. SHARMA, K.K. SHARMA, A. KUMAR, *Surface waves in a piezoelectric-semiconductor composite structure*, International Journal of Solids and Structures, **47**, 6, 816–826, 2010.

26. C.L. GU, F. JIN, *Shear-horizontal surface waves in a half-space of piezoelectric semiconductors*, Philosophical Magazine Letters, **95**, 2, 92–100, 2015.

27. X.S. CAO, S.M. HU, J.J. LIU, J.P. SHI, *Generalized Rayleigh surface waves in a piezoelectric semiconductor half space*, Meccanica, **54**, 12, 271–281, 2019.

28. F.Y. JIAO, P.J. WEI, X.L. ZHOU, Y.H. ZHOU, *The dispersion and attenuation of the multi-physical fields coupled waves in a piezoelectric semiconductor*, Ultrasonics, **92**, 68–78, 2018.

29. V.J. GOKHALE, M. RAIS-ZODEH, *Phonon-electron interactions in piezoelectric semiconductor bulk acoustic wave resonators*, Scientific Reports, **4**, 5617, 2014.

30. I. BEN SALAH, F. TAKALI, C. OTHMANI, A. NJEH, *SH wave in a stressed piezoelectric semiconductor plates: Electron and hole drift phenomenon*, International Journal of Mechanical Sciences, **223**, 107281, 2022.

31. R. TIAN, J.X. LIU, E.N. PAN, Y.S. WANG, A.K. SOH, *Some characteristics of elastic waves in a piezoelectric semiconductor plate*, Journal of Applied Physics, **126**, 12, 125701, 2019.

32. D.Z. LI, S.P. LI, C.L. ZHANG, W.Q. CHEN, *Propagation characteristics of shear horizontal waves in piezoelectric semiconductor nanoplates incorporating surface effect*, International Journal of Mechanical Sciences, **247**, 108201, 2023.

33. Z.B. Wei, P.J. Wei, C.Y. Xu, X. Guo, *Equivalent imperfect interface model of PN junction of piezoelectric semiconductor for the multi-field coupled waves propagation*, Acta Mechanica, **235**, 1, 73–92, 2024.

34. L. Elmaimouni, J.E. Lefebvre, V. Zhang, T. Gryba, *A polynomial approach to the analysis of guided waves in anisotropic cylinders of infinite length*, Wave Motion, **42**, 2, 177–189, 2005

35. A. Boström, M. Golub, *Elastic SH wave propagation in a layered anisotropic plate with interface damage modelled by spring boundary conditions*, Quarterly Journal of Mechanics and Applied Mathematics, **62**, 1, 39–52, 2008.

36. X.M. Zhang, J.G. Yu, *Effects of initial stresses on guided waves in unidirectional plates*, Archives of Mechanics, **65**, 1, 3–26, 2013.

37. P. Ernian, W.Q. Chen, *Static Green's Functions In Anisotropic Media*, Cambridge University Press, New York, USA, 2015.

Received February 3, 2025; revised version June 27, 2025.
Published online August 20, 2025.